Size Effects on the Photophysical Properties of Colloidal Anatase TiO2 Particles: Size Quantization Versus Direct Transitions in This Indirect Semiconductor?

ARTICLE *in* THE JOURNAL OF PHYSICAL CHEMISTRY · NOVEMBER 1995

Impact Factor: 2.78 · DOI: 10.1021/j100045a026

3 AUTHORS, INCLUDING:

Nick Serpone
University of Pavia
435 PUBLICATIONS **17,891** CITATIONS
SEE PROFILE

Darren Lawless
Sheridan College (Oakville)
38 PUBLICATIONS **2,269** CITATIONS
SEE PROFILE

Size Effects on the Photophysical Properties of Colloidal Anatase TiO_2 Particles: Size Quantization or Direct Transitions in This Indirect Semiconductor?

N. Serpone,* D. Lawless,† and R. Khairutdinov‡

Center for Fast Laser Spectroscopy and the Laboratory of Pure and Applied Studies in Catalysis, Environment and Materials, Department of Chemistry and Biochemistry, Concordia University, Montreal, Quebec, Canada H3G 1M8

Received: January 31, 1995; In Final Form: August 20, 1995[⊗]

Colloidal TiO_2 sols with average particle size $2R_p$ = 2.1 nm (specimen A), 13.3 nm (specimen B), and 26.7 nm (specimen C) were prepared and characterized by absorption and photoluminescence spectroscopies. Electron and X-ray diffraction examination showed the specimens contain anatase as the only crystalline phase (~20−30%) and a significant amorphous component (~70−80%). The three specimens gave identical steady-state absorption features at high loadings. Luminescence around 340−350 nm (at the absorption edge at the lower loadings) was more intense in the 13.3 nm TiO_2 particles; several weaker bands were seen at longer wavelengths. Congruence of the absorption onsets for the three specimens at 15 g L^{-1} or at the lower loadings (0.015 and 0.30 g L^{-1}) argues against size quantization effects for particles with $R_p \geq 1.0$ nm. Spectra at the lower loadings exhibited absorption thresholds at considerably higher energy (relative to bandgap); they are attributed to direct transitions in an otherwise indirect bandgap TiO_2 semiconductor. Considerations of the effective mass model to determine particle size from spectral blue shifts of absorption edges and to ascertain size quantization in semiconductor colloidal particles suggest that it is rather premature to reach any conclusion on size quantization manifestations in the absence of a precise knowledge of the effective masses of charge carriers in small nanosized particles, and more so for anatase colloids for which inferences of effective masses of electrons and holes have been taken from rutile bulk crystals.

Introduction

Application of semiconductor systems to initiate and control various photocatalytic processes[1] has stimulated interest in elucidating the photophysical properties of semiconductor colloids, together with the dynamics of interfacial processes at the semiconductor/electrolyte interface.[2−7] Understanding these properties in semiconductor materials is therefore of particular interest in heterogeneous photocatalysis. Of great import is the understanding of the photophysical behavior of TiO_2 in aqueous media because of its extensive application in the detoxification of polluted ecosystems. As well, TiO_2 is used extensively as the whitening agent in paints in which photoinduced charge carrier processes are known to play a role in their degradation.[8]

Particle size has pronounced effects on the spectral properties of semiconductors when their size becomes comparable with the size of the exciton (the so-called Q-size effect); a number of semiconductors, e.g., CdS,[9] ZnS,[10] and AgI,[11] have shown spectral blue shifts in the absorption band edge as a consequence of exciton confinement with decreasing particle size. Particle size also has a pronounced effect on the charge carrier dynamics in semiconductor particulates.[11] Several studies concerning the photophysics of TiO_2 colloids have been reported.[4,12−17] A few recent accounts[18−23] have claimed exciton confinement and thus Q-size effects in very small TiO_2 colloid particles in the size range 1.0−12.0 nm. Systematic studies of the dependence of the photophysical properties of TiO_2 sols on particle size have not kept pace with studies in heterogeneous photocatalysis where TiO_2 plays a significant role.

Anpo and co-workers[21] reported particles of rutile and anatase titania with size (expressed as $2R_p$, where R_p is the particle radius) in the range 5.5−200 nm (rutile) and 3.8−53 nm (anatase). Apparently, these crystallites displayed distinct size quantization effects even at such relatively large sizes. For a 12 nm rutile particle the bandgap increased by ~0.067 eV relative to the bulk bandgap (3.03 eV); for anatase particles the bandgap increased by about 0.156 eV relative to the bulk value of 3.18 eV. The bandgap was determined from the threshold of the absorption edge of these microcrystallites. Photocatalytic activity of both rutile and anatase increased with increase in the BET surface area and with the magnitude of the blue shift in the bandgap.[21] The greater reactivity of the two TiO_2 polymorphs seems to be due mostly to modifications in the electronic properties of the smaller particulates.

Kormann and co-workers indicated that the small particles of TiO_2, prepared using the arrested hydrolysis of either titanium tetrachloride[18] or tetraisopropoxide,[23] show size quantization when $2R_p$ = 2.0−4.0 nm. The particles exhibited a 0.15−0.17 eV blue shift of the optical absorption edge under anaerobic illumination. They assigned the shift to exciton confinement in these otherwise very small particles. Others[20] inferred that the shift of the bandgap to higher energies, also exhibited by particle sizes in the range 2.5 nm $\leq R_p \leq$ 10.0 nm,[24−29] was likely due to a Burstein−Moss (B−M) effect (i.e., the band-filling mechanism).[30] However, at spectrophotometric light intensities normally used to record absorption spectra the B−M effect should be of little consequence. Blue shifts in bandgap of ~0.1 eV were reported by Kavan et al.[20] for extremely small particles of TiO_2 ($2R_p$ = 1.0−2.0 nm) prepared by oxidative hydrolysis of $TiCl_3$. They attributed the shift of the absorption edge to size quantization as low-intensity illumination was used to minimize the significance of the Burstein−Moss effect. Joselevich and Willner[22] reported the absorption edge in TiO_2

† Present address: Sterling Pulp Chemicals, Ltd., Toronto, Canada.
‡ Visiting Professor, 1994−1995. Permanent address: Institute of Chemical Physics, Academy of Sciences of Russia, ul. Kosygina 4, 117 334 Moscow, Russia.
* All correspondence to this author at Concordia University.
[⊗] Abstract published in *Advance ACS Abstracts*, October 15, 1995.

0022-3654/95/2099-16646$09.00/0

particles prepared in a water-in-oil microemulsion to be at 3.6 eV (blue shift ~0.4 eV if the particles were anatase and about 0.6 eV if rutile). A particle size of $2R_p = 1.5$ nm for anatase and 1.2 nm for rutile was estimated. The absorption onset did not change on dilution from 0.5 to 0.1 g L^{-1}.

For a semiconductor particle displaying size quantization, the increase in bandgap energy ΔE_{BG} is, to a first approximation, a function[7] (eq 1) of the radius of the particle (R_p), the effective mass of the exciton μ (where $\mu^{-1} = m_e^{-1} + m_h^{-1}$; m_e and m_h are the effective masses of the electron and hole, respectively), and the dielectric constant of the semiconductor material:

$$\Delta E_{BG} = h^2/8R_p^2\mu - 1.8e^2/4\pi\epsilon_0\epsilon R_p \qquad (1)$$

The change in bandgap energy, ΔE_{BG}, is thus expected to depend critically on the reduced effective mass of the charge carriers, which for the TiO_2 electrons has been taken to range from $5m_0$ to $13m_0$[31-33] and m_h to be $\sim 2m_0$[18] and $\geq 3m_0$;[34] elsewhere, m_e was taken as $30m_0$[3,35] and as $0.01m_0$.[36] Clearly, the precise values of the effective masses of electrons and holes in TiO_2 remain elusive for single crystals of rutile and even more so for anatase TiO_2 particles. Exciton radii R_{exc} between 0.75 and 1.9 nm were estimated for small titania particles[18] by the relation[7] $R_{exc} = \epsilon a_0 m_0/\mu$, where $\epsilon = 184$ for TiO_2,[18] m_0 is the electron rest mass, and a_0 is the Bohr radius of the H atom (0.529 Å). Gratzel[3] estimated R_{exc} to be ~0.3 nm if contributions from valence band holes were neglected. Estimations using $m_e = 0.01m_0$[36] give $R_{exc} \sim 1$ μm. Hence, TiO_2 particles should display a size quantization threshold at $2R_p \leq 0.6$ nm according to some workers[3] and at $2R_p \leq 1.5-3.8$ nm according to others,[18] and even at $2R_p \leq 2$ μm if $m_e = 0.01m_0$ were used.[36] Note therefore how predictions of thresholds of Q-size effects depend critically on the estimate of m_e and even more so on m_h since $m_h \ll m_e$.

The expression for ΔE_{BG} (eq 1) has been used extensively to estimate the size of small semiconductor particles, often corroborated by transmission electron microscopy. This congruence notwithstanding, there are other plausible explanations for the observed blue shifts in bandgap. We have addressed this issue of size effects on semiconductor photophysics of naked and doped TiO_2 specimens;[37] the latter studies will be reported at a later date.

This paper reports the absorption and photoluminescence features of nanosized (2.1, 13.3, and 26.7 nm diameter) TiO_2 colloidal particles (henceforth referred to as specimens A, B, and C, respectively). We argue that there are no size quantization effects on the spectral properties of TiO_2. Rather, the results presented below indicate that so-called Q-size effects[18-23] from spectral blue shifts in absorption spectra of solutions of TiO_2 colloidal particles are the result of *direct interband transitions* in an otherwise indirect bandgap semiconductor. The particle sizes examined seem to affect the charge carriers relaxation dynamics; they are not related to exciton confinement. We report on this elsewhere.[38]

Experimental Section

All chemicals were of reagent grade quality; the water was doubly distilled and deionized. Clear and optically transparent colloidal sols of TiO_2 were prepared by the low-temperature controlled hydrolysis of $TiCl_4$.[39]

In a typical preparation, 5.2 mL of fresh doubly distilled $TiCl_4$ was slowly added dropwise to 200 mL of water maintained at ~0 (±0.2) °C under vigorous stirring. Following dialysis (Viscase membrane, presoaked for 24 h in distilled water and then thoroughly rinsed prior to use) against ~4 L of distilled water (replaced several times) for about 8 h, the resulting TiO_2 sol concentration was 15 g L^{-1} and the pH ranged between 2.5 and 3 (dependent on the length of dialysis and the concentration of TiO_2 prepared).

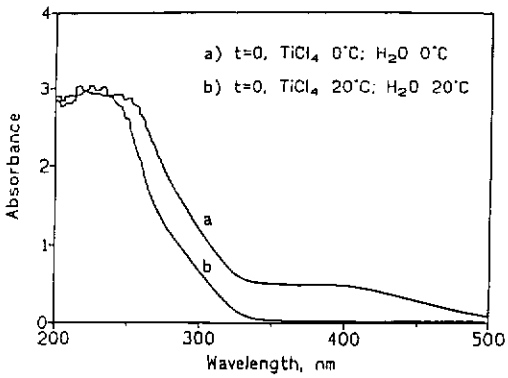

Figure 1. Steady-state absorption spectral changes when (a) $TiCl_4$ (0 °C) is initially added to water and then (b) allowed to warm to ~20 °C. (Unless noted otherwise, these spectra and elsewhere represent absorption spectra of colloidal sols.)

The size of TiO_2 particles was controlled by careful manipulation of the temperature of either the $TiCl_4$ or the water to which $TiCl_4$ was added. Very small TiO_2 particles (diameter about 2.0 nm) were produced when the above procedure was used but with $TiCl_4$ maintained at −20 °C. Cooling was provided by a Model K4R Lauda constant temperature bath (50/50 mixture of ethylene glycol/water). On reaching −20 °C, the $TiCl_4$ flask was equilibrated for ~30 min prior to synthesis start-up. Raising the temperature of $TiCl_4$ from 0 to 24, 44, and 66 °C, while maintaining the water at 0 °C, had no significant effect on the average particle diameter. However, the temperature of water significantly affected the particle size. Thus, when $TiCl_4$ was added at ambient temperature to water maintained at 10 °C, the average particle diameter (dynamic light scattering) was ~27 nm. If $TiCl_4$ were added to water at 24 °C, the colloidal sol was unstable and precipitated within a few hours.

Powder X-ray diffraction patterns of TiO_2 specimens were obtained with a Philips PW 1050−25 diffractometer using Ni-filtered Kα radiation of copper ($\lambda = 1.5417$ Å). The powder was obtained from slow air-drying of the colloid followed by grinding with a mortar and pestle and later placed in a flat holder made of Plexiglas. The presence of a single crystalline anatase phase was confirmed by electron diffraction. Transmission electron microscopic examination of the TiO_2 samples was carried out on a Philips EM 420 instrument. UV/vis spectra were recorded either on a Shimadzu UV-265 double-beam recording spectrophotometer or on a Varian 2300 spectrophotometer using 1 cm Suprasil quartz cells; distilled water (pH 3, adjusted using HCl) was the reference. Diffuse reflectance measurements were done on the Shimadzu UV-265 spectrophotometer fitted with a P/N 204-05857 integrating sphere reflectance unit. Fluorescence spectra were obtained on a Perkin-Elmer MPF-44B spectrofluorimeter equipped with a Corning 0−54 filter.

Results and Discussion

Growth of TiO_2 Particles. Figure 1 illustrates the spectral changes immediately observed when $TiCl_4$ was added to water. Initially, a broad absorption band formed around 400 nm which was most pronounced when the initial temperature of the $TiCl_4$ was 0 °C; it also appeared when ambient temperature $TiCl_4$ was added to cold water. On warming to ~20 °C, the band disappeared, and the only absorption observed was the band edge absorption of the growing TiO_2 particles.

The initial absorption band at 400 nm indicates that formation of colloidal TiO_2 is more complex than simple hydrolysis of $TiCl_4$ (eq 2) would indicate, and although hydrolysis of titanium(IV) compounds has been studied extensively, a number of uncertainties remain concerning the nature of the protolysis products.[40] The preparative methods of semiconductor materials affect their properties.[41] The early stages of particle growth should also impact somewhat on the ultimate photophysical and photocatalytic properties of TiO_2.

$$TiCl_4 + 2H_2O \rightarrow TiO_2 + 4H^+_{aq} + 4Cl^- \qquad (2)$$

Under highly acidic conditions (0.5 M $\leq$ $[H^+]$ $\leq$ 2 M) and high concentration of Cl^- ions, the species $(H_2O)_5Ti(OH)^{3+}\cdot 3Cl^-$ and $(H_2O)_4Ti(OH)_2^{3+}\cdot Cl^-$ are formed in detectable quantity.[40] We infer that the ~400 nm band arises from a ligand (chloride)-to-metal charge transfer transition.[42] This assignment accords with recent observations by Serpone and Kennepohl,[43] who spectrally examined a mixture of $TiCl_4$ in relatively dry (<1% water) ethanol; a highly intense band also formed in the same spectral region. Given the insufficient quantity of water to cause complete hydrolysis of $TiCl_4$, the absorption band was attributed to a Cl^- to Ti^{IV} charge transfer transition.

Rapid spectral changes occur during the first 3 h of preparation of the 15 g L^{-1} TiO_2 sols (all three specimens), after which no further absorption spectral changes were noted. During dialysis, the pH of the sol increased from 0.1 (t = 0) to 2.6 (t = 8 h). The most rapid pH changes occurred during the first 3 h which when taken together with the spectral observations infer that particle growth had terminated by this time.

Temporal spectral changes were examined in greater detail during the preparation of more dilute colloidal TiO_2 sols.

(i) The 13.3 nm TiO_2 Particles. The spectral changes illustrated in Figure 2a for 0.3 g L^{-1} TiO_2 did not exhibit the normal Beer–Lambert behavior; no further spectral changes were discernible after 30 min. The inset shows that formation of small titania clusters, $(TiO_2)_n$, the building blocks of the final $(TiO_2)_N$ lattice, occurred almost immediately on addition of $TiCl_4$ to the water (absorption at t = 0). During the next 20 min, the absorbance increased linearly and then plateaued (t = 30 min) at the maximal particle growth. The overall nonlinear increase in absorbance suggests that aging is one of particle growth and not of an increase in the concentration of the chromophoric species. The agglomeration of $(TiO_2)_n$ clusters was constant from 0 to 20 min; in the ensuing 10 min, whatever changes occurred in the nature of the sols arrested further particle growth.

(ii) The 2.1 nm TiO_2 Particles. The temporal absorption changes during the formation of 2.1 nm TiO_2 particles (0.3 g L^{-1}) are shown in Figure 2b. The inset summarizes the absorbance changes at 340 nm over the first 50 min; after this time there were no additional observable spectral changes. Though the growths of the 2.1 and 13.3 nm TiO_2 sols are spectrally similar, the time required to form the smaller $(TiO_2)_N$ particulates was longer (ca. 50 min) than for the larger sols (30 min). A different behavior was also noticeable in the early growth stages of the 2.1 nm particles: the absorbance changes were nonlinear in the first 10 min. We infer that during this period the low temperature of the $TiCl_4$ (−20 °C) led to formation of other (but unknown) chlorohydroxotitanium(IV) species which ultimately transformed into additional $(TiO_2)_n$ clusters. During the ensuing 40 min, diffusion and agglomeration of the $(TiO_2)_n$ units controlled the microcrystallites growth process.

(iii) The 26.7 nm TiO_2 Particles. The growth of the 26.7 nm particles was very rapid; no spectral changes were discernible after 10 min, inferring that complete hydrolysis had occurred immediately on addition of $TiCl_4$ to the water at 10 °C.

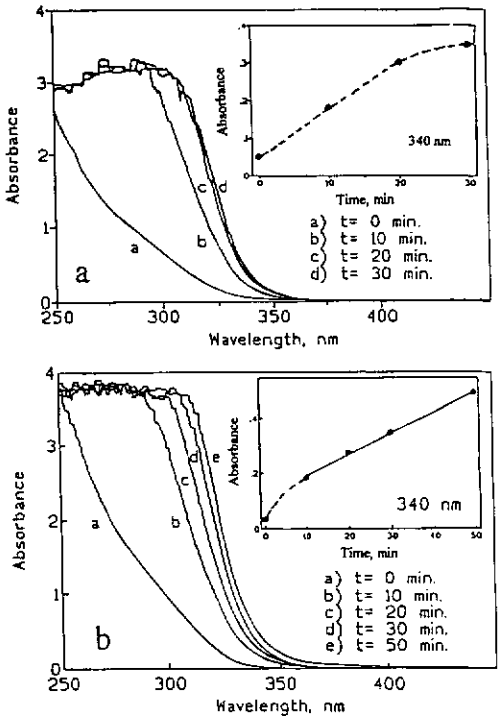

Figure 2. Changes in absorption spectra of (a) 13.3 nm TiO_2 particles and (b) 2.1 nm TiO_2 particles with time during the early stages of synthesis (TiO_2, loading 0.3 g L^{-1}; optical path length, 1 cm).

We infer from the above that the nature and the existence of intermediates formed during the hydrolysis process must be dependent on the temperatures of both reacting species (reaction 2), and their concentration in some way may determine the formation of defects and traps in the TiO_2 lattice. These intermediates were not examined further in the present study.

(iv) Determination of Size and Form of the TiO_2 Particulates. The mean particle size of the three TiO_2 specimens was determined by dynamic light scattering (Figure 3); the mean specimen sizes were $2R_p$ = 2.1 nm (specimen A), $2R_p$ = 13.3 nm (specimen B), and $2R_p$ = 26.7 nm (specimen C). The sizes of the particulates are characterized by the width of the Gaussian size distribution ±1.1 nm (specimen A), ±4.5 nm (specimen B), and ±9.0 nm (specimen C). The morphology and particle size were also examined by transmission electron spectroscopy (TEM). The particles are nearly spherical. Analysis of particle size distributions from several TEM photographs of specimen B gave $2R_p$ = 8.4 ± 2.8 nm, in fair accord with the hydrodynamic radius from the light scattering experiments. Particle sizes in the ~1 nm regime are somewhat difficult to determine and inherently carry some error.

Electron diffraction examination of TiO_2 specimen B showed that the only crystalline phase present was anatase. This was corroborated by X-ray diffraction examination of the same sample whose pattern is presented in Figure 4a; for comparison, Figure 4b illustrates the pattern for Degussa TiO_2 P-25, which consists of ~80% anatase and ca. 20% rutile.[41] The latter titania sample is highly crystalline (mean crystallite size ~30 nm) as witnessed by the sharp and intense peaks. By contrast, the X-ray pattern of specimen B shows weak and very broad signals, suggesting that sample B consists of rather small particles; the pattern of Figure 4b infers a size $2R_p$ ~ 3.6 nm (versus 13.3 nm; see above). Various factors affect the relative intensities of diffracted peaks,[44] but to the extent that for a pattern to be discernible the sample must constitute at least 5% crystalline

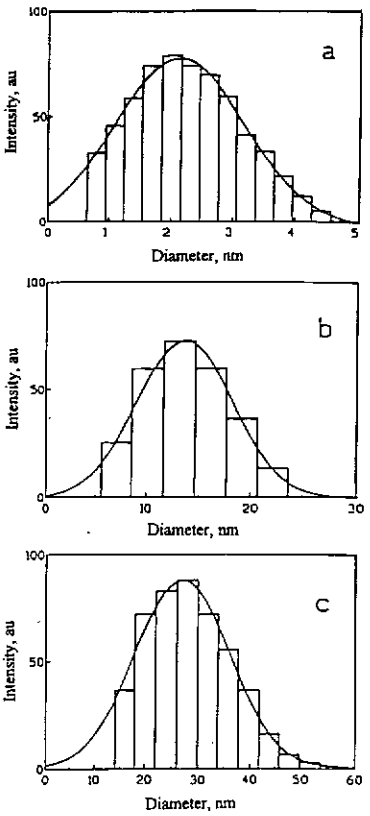

Figure 3. Particle size distribution of (a) specimen A ($2R_p = 2.1$ nm) TiO_2, (b) specimen B ($2R_p = 13.3$ nm) TiO_2, and (c) specimen C ($2R_p = 26.7$ nm) TiO_2 (loading of TiO_2, 0.3 g L^{-1}).

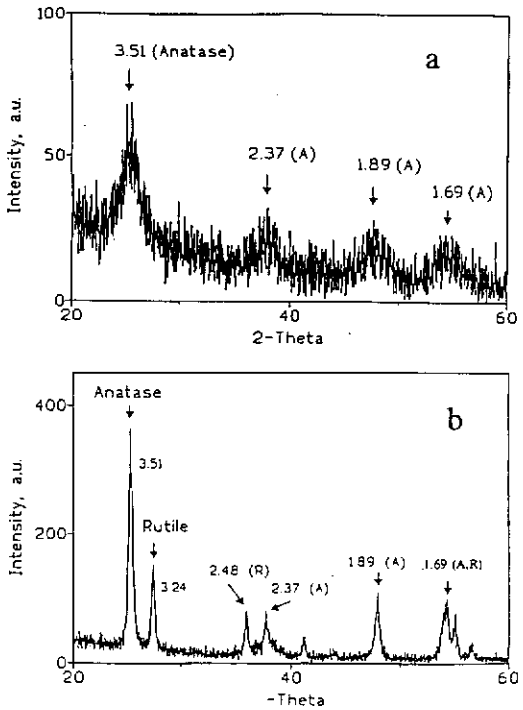

Figure 4. (a) X-ray diffraction pattern of a sample of specimen B TiO_2; the numbers correspond to calculated d spacings, and the peaks are those of the anatase crystalline form. (b) X-ray diffraction pattern of a sample of Degussa TiO_2 P-25 taken for comparison (see text); the numbers refer to the d spacings, and A and R refer to anatase and rutile forms of titania.

material,[45] we conclude that sample B may have a nonnegligible amorphous component[39] (~70–80% amorphous and ~20–30% anatase), contrary to a recent report[46] in which the 2.0–4.0 nm TiO_2 particles were completely in the anatase form.

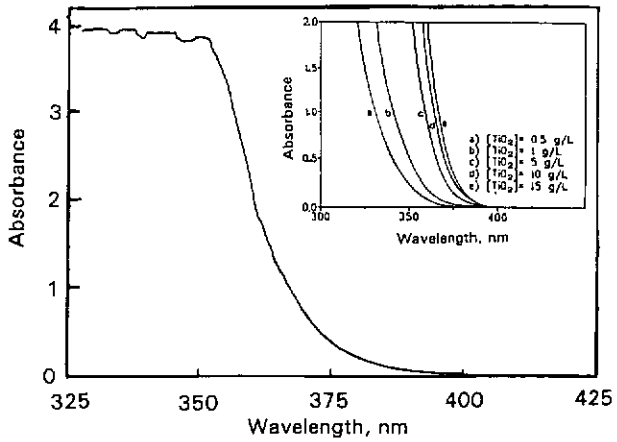

Figure 5. Steady-state absorption spectra of specimens A, B, and C colloidal TiO_2 particles (TiO_2 loading, 15 g L^{-1}; optical path length, 1 cm). All spectra are identical. The inset shows the absorption spectra of specimen B at various loadings (pH = 2.7); the absorbances at 370 nm follow a Beer–Lambert behavior.

Absorption Spectra of Colloidal TiO_2 Particles. Absorption spectra of the TiO_2 sols A, B, and C are shown in Figure 5; loadings were 15 g L^{-1}. The three spectra are identical and correspond to the absorption spectrum of bulk anatase TiO_2; they are also in good agreement with the spectra of colloidal TiO_2 (12.0 nm diameter) reported earlier.[18,19,39] The insert in Figure 5 illustrates the concentration dependence of the spectra of specimen B from 0.5 to 15 g L^{-1}; absorption changes follow a Beer–Lambert behavior, indicating no aggregation took place at the higher loadings.

That the three spectra are identical and display no blue shifts in the UV–vis spectra, normally associated with decreasing particle size, was not totally unexpected. Although the spectral results of Figure 5 are in keeping with the predictions of Gratzel[3] (blue shift of the absorption band edge threshold below $2R_p = 0.6$ nm), they differ from a recent study[18] in which 2.0 nm diameter TiO_2 particles (~200 molecules of TiO_2[19]) showed an apparent increase in bandgap of ~0.15 eV relative to bulk TiO_2 (see ref 47). Our observations on the TiO_2 specimens indicate that the bandgap energies of these particles, determined by extrapolation to zero absorption coefficients α, are identical (~3.18 eV; see below); α was assessed for the three specimens from eq 3[48]

$$\alpha = 2.303 \times 10^3 A\varrho/lc \qquad (3)$$

where A is the sample absorbance, ϱ is the TiO_2 density, 3.84 g cm^{-3}, c is the loading of the colloid in g L^{-1}, and l is the path length.

Estimates of the bandgap energies for the three small particle specimens were also done by diffuse reflectance spectra after the colloids had been dried.[48] The resulting spectra were identical to each other and identical with the absorption features of Figure 5. We now examine the optical properties of the three TiO_2 specimens.

Note at first that semiconductors are classified as direct or indirect semiconductors according to the nature of the lowest allowed electronic transition. Direct semiconductors are characterized by the minimum of the lowest conduction band positioned in **k** space directly under the maximum of the highest valence band. The optical absorption coefficient α near the absorption edge for *direct* interband transitions is given by eq 4[49]

$$\alpha = B_d(h\nu - E_g)^{1/2}/h\nu \qquad (4)$$

where B_d is the absorption constant for a direct transition.

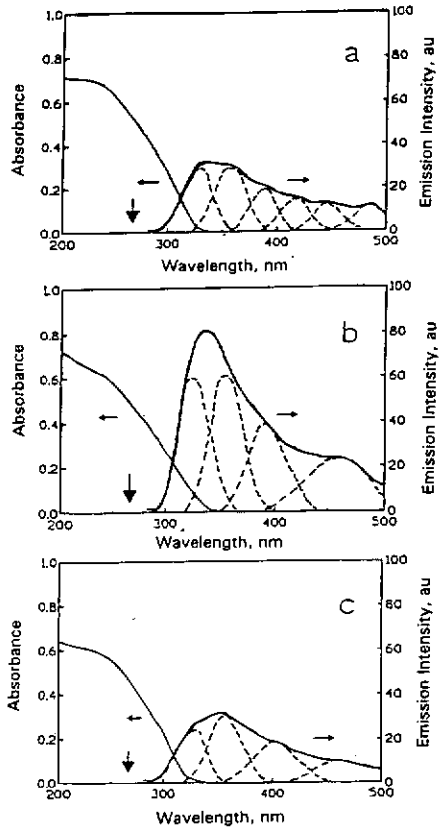

Figure 6. Absorption and fluorescence spectra of (a) specimen A, (b) specimen B, and (c) specimen C colloidal TiO_2 particles. TiO_2 loading, 0.015 g L^{-1} for (a, b) and 0.3 g L^{-1} for (c); pH 2.7 in all cases; excitation wavelength, 270 nm (see arrow).

For indirect semiconductors, the minimum of the lowest conduction band is shifted relative to the maximum of the highest valence band, and the lowest-energy interband transition must then be accompanied by phonon excitation. Indirect interband transitions are characterized by the stronger energy dependence of the optical absorption coefficient α nearer the absorption edge than is otherwise the case for direct transitions[49,50]

$$\alpha = B_i(h\nu - E_g)^2/h\nu \qquad (5)$$

where B_i is the absorption constant for an indirect transition.

For indirect transitions in TiO_2, a plot of $(\alpha h\nu)^{1/2}$ versus $E\{h\nu\}$ from the spectra of specimens A, B, and C gave two straight lines whose intercepts (i.e., onset of absorptions; see Figure 7a below; estimated error in energies $\leq \pm 0.05$ eV, correlation coefficients $\geq 99.8\%$) occur at ~2.97 and ~3.21 eV; the latter is ascribed to the bandgap absorption edge of anatase titania (see below). Moser[39] reported similar values for 12.0 nm and inferred that these larger than theoretically predicted values[51] are caused by lattice contraction of the TiO_2 particle because of a significant pressure produced by the surface tension (about 1%) as illustrated by a V^{4+}-doped TiO_2 sample.[52] Our present findings show that specimens A, B, and C possess bulk anatase bandgaps, and we thus infer that there is no size quantization in the size regime $2R_p > 2.0$ nm for TiO_2 particles, contrary to earlier reports.[18,21,23]

A 1000-fold dilution of TiO_2 specimens A and B (15 to 0.015 g L^{-1}) gave the absorption spectra illustrated in Figure 6a,b. At 0.015 g L^{-1}, the average number of microcrystallites with $2R_p = 26.7$ nm in a solution of specimen C that will interact with a single light quantum in the cell of path length $l = 1$ cm is about 2. Light absorption at such a small concentration of

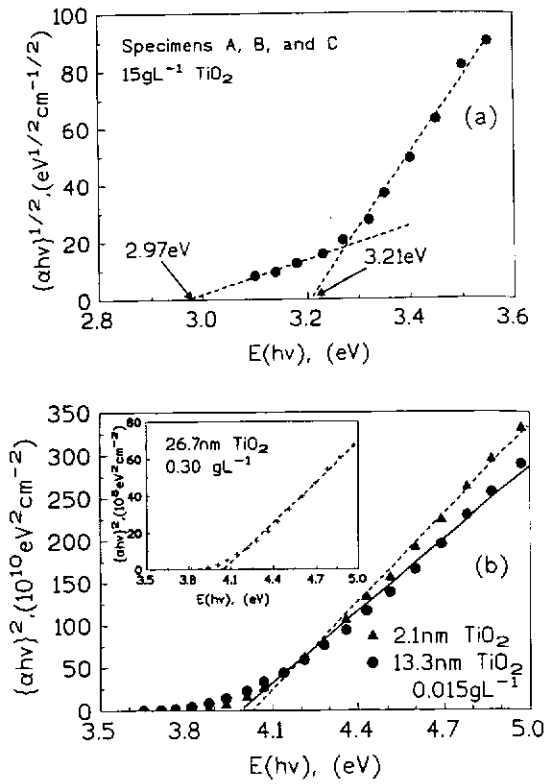

Figure 7. (a) Plots of $(\alpha h\nu)^{1/2}$ versus $E\{h\nu\}$ for specimen A, B, and C colloidal TiO_2 particles (TiO_2 loading, 15 g L^{-1}). Absorption coefficients α are form the steady-state absorption spectra in Figure 5. (b) Plots of $(\alpha h\nu)^2$ versus $E\{h\nu\}$ for specimen A, B, and C (insert) at loadings of 0.015, 0.015, and 0.30 g L^{-1}, respectively (estimated error of the energy—X intercept—$\leq \pm 0.05$ eV; correlation coefficients, $\geq 99.8\%$).

absorbers is lower than that predicted by the Beer–Lambert law, and an absorption spectrum for specimen C identical to those depicted in Figure 6a,b was obtained only at a concentration of 0.30 g L^{-1}. Equal absorption conditions at $\lambda_{ex} = 270$ nm were needed to compare the emission behavior fo the three specimens (see below). Plots of $(\alpha h\nu)^{1/2}$ versus $E\{h\nu\}$ from the spectral data of Figure 6 displayed no linear relationships between 250 and 340 nm as were expected for the lowest interband transition in the indirect semiconductor TiO_2. By contrast, linear relationships obtained only when absorption coefficient data were plotted as $(\alpha h\nu)^2$ versus $E\{h\nu\}$ at $\lambda \leq$ 340 nm (Figure 7b). Thus, the stronger absorption features in Figure 6 are those of *allowed direct band transitions* in an otherwise indirect bandgap semiconductor. The intercepts in the plots of Figure 7b place these (direct) Franck–Condon type transitions at 4.04 eV (307 nm, specimen A) and 4.03 eV (308 nm) for specimens B and C. Within experimental error, these values denote the same electronically allowed direct transition.

The small absorption tails at longest wavelength show an onset at 3.68, 3.61, and 3.68 eV for A, B, and C, respectively.

Spectral Assignments. Rutile and anatase TiO_2 possess structures which exhibit distorted TiO_6 octahedra, the basic constituents of many perovskite ferroelectrics.[53] For the rutile polymorph there are small differences between single crystals and polycrystalline materials insofar as mobility, effective mass, and thermal activation energy of charge carriers are concerned.[54] In TiO_2 and other metal oxides (e.g., $SrTiO_3$, $BaTiO_3$), a separation of ~15 eV between filled oxygen 2p and empty Ti 3d levels seems typical when such oxides are fully ionic. Bandgaps of much lower energies (e.g., 3.0 V for rutile and 3.2 V for anatase) infer a departure from full ionicity,[55] as the 2p–3d separation is sensitive to the degree of ionic versus

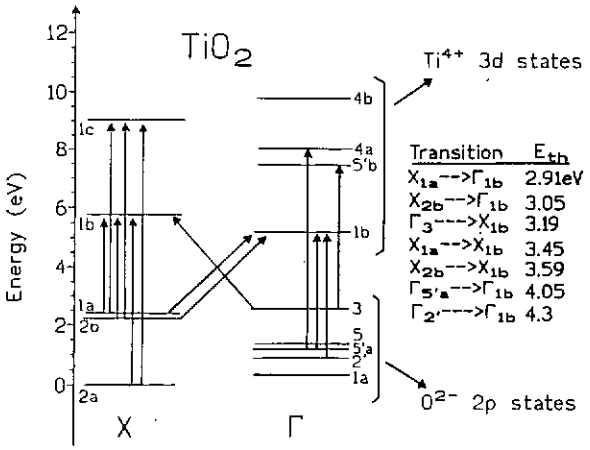

Figure 8. Short energy level diagram illustrating the relative energy levels in TiO_2 as calculated by Daude et al.[51] The arrows indicate a few of the allowed direct and indirect transitions. The level X_{2a} positioned at zero energy for the sake of simplicity.

TABLE 1: Energies of Direct and Indirect Transitions in a TiO_2 Semiconductor

		energy, eV		
transition[a]	nature	calculated[b]	experimental bulk crystals	experimental, particles
$X_{1a} \rightarrow \Gamma_{1b}$	indirect	2.91	3.026[c]	2.97[g]
$X_{1b} \rightarrow \Gamma_{1b}$	indirect	3.05	3.029,[c] 3.059[d]	2.97[g]
$\Gamma_3 \rightarrow X_{1b}$	indirect	3.19	3.114,[c] 3.13[d]	3.21[g] (3.10)[i]
$X_{1a} \rightarrow X_{1b}$	direct	3.45	3.3[e]	3.61−3.68[g] (3.44)[i]
$X_{2b} \rightarrow X_{1b}$	direct	3.59	3.4[e]	3.61−3.68[g]
$\Gamma_{5'a} \rightarrow \Gamma_{1b}$	direct	4.05	4.0,[f] 4.07[e]	4.03−4.04[g]
$\Gamma_{2'} \rightarrow \Gamma_{1b}$	direct	4.3	4.11,[f] 4.15[e]	

[a] See Figure 8. [b] Reference 51. [c] Reference 56. [d] Reference 57. [e] Reference 58. [f] Reference 60. [g] This work. [i] Reference 36.

covalent character in the bonding. These ideas have been exploited to clarify the properties of a variety of n-type transition metal oxide semiconductors.

The electronic band structure of TiO_2 was reported by Daude and co-workers.[51] Titania possesses a highly ionic lattice[55] with the valence band composed principally of oxygen 2p orbitals, with the corresponding wave functions considerably localized on the O^{2-} lattice sites. The conduction band consists mostly of excited states of Ti^{4+}. The width of the O^{2-} 2p valence bands is about 16 eV; the breadth of the 3d conduction bands is ~27 eV.[51] A short modified energy level diagram is depicted in Figure 8 where X denotes the edge and Γ the center of the Brillouin zone (BZ); see also Table 1. The two lowest-energy vertical (direct) transitions, $\Gamma_3 \rightarrow \Gamma_{1b}$ and $\Gamma_5 \rightarrow \Gamma_{1b}$, at the BZ center are forbidden. The lowest energy *allowed phonon-assisted transitions* are the indirect transitions from the edge to the center of the Brillouin zone, namely $X_{1a} \rightarrow \Gamma_{1b}$ (2.91 eV) and $X_{2b} \rightarrow \Gamma_{1b}$ (3.05 eV), which accord with the experimental values 3.03 and 3.06 eV, respectively.[56,57] The theoretically estimated transition from the center to the BZ edge $\Gamma_3 \rightarrow X_{1b}$ (3.19 eV) is in keeping with the experimentally observed transitions at 3.11 and 3.13 eV.[56,58] The first *allowed vertical* transitions occur at the X edge of the Brillouin zone: $X_{1a} \rightarrow X_{1b}$ (3.45 eV) and $X_{2b} \rightarrow X_{1b}$ (3.59 eV), in agreement with the experimental observations by Frova et al.[58] (transitions at 3.3 and 3.4 eV, respectively); the next lowest-energy allowed direct transitions are $\Gamma_{5'a} \rightarrow \Gamma_{1b}$ (4.05 eV) and $\Gamma_{2'} \rightarrow \Gamma_{1b}$ (4.3 eV).[51]

The above discussion and the theoretical predictions of Daude and co-workers[51] permit some assignments for the absorption thresholds of various transitions in the TiO_2 specimens A, B, and C; they are summarized in Table 1. Our observation of the lowest-energy absorption threshold at 2.97 eV is not precise enough to distinguish the nearly degenerate indirect transitions $X_{1a} \rightarrow \Gamma_{1b}$ and $X_{2b} \rightarrow \Gamma_{1b}$; earlier studies[56,57] placed these transitions at ~3.03−3.06 eV. The onset of absorption at 3.21 eV corresponds to the bandgap energy of anatase and is ascribed to the indirect transition, $\Gamma_3 \rightarrow X_{1b}$, predicted to occur at 3.19 eV (Figure 8). The two lowest-energy, also nearly degenerate but direct, transitions take place in the X zone ($X_{1a} \rightarrow X_{1b}$ and $X_{2b} \rightarrow X_{1b}$) at 3.61−3.68 eV for the three specimens examined. For rutile TiO_2 (bandgap ~3.0 eV) the onset of absorption of the lowest-energy *direct transition* was reported at 3.2 eV.[59] The first allowed direct transition at the center of the zone for anatase, namely $\Gamma_{5'a} \rightarrow \Gamma_{1b}$, is seen in all three specimens at 4.03−4.04 eV; it was predicted at 4.05 eV[51] and observed at 4.0[60] and at 4.07 eV[55] for bulk TiO_2 crystals. Our conditions did not allow us to probe higher-energy transitions.

Analogous observations of direct transitions in TiO_2 and in other indirect bandgap semiconductors were also reported long ago by physicists[51,58,60] and more recently by Wold and co-workers[61] for $SrTiO_3$, $Sr_{0.5}Ba_{0.5}Nb_2O_6$, WO_3, and Fe_2O_3.

Luminescence of Colloidal TiO_2 Specimens. Electronic transitions in semiconductors must conserve momentum; photon momentum is very low. Indirect transitions, therefore, implicate simultaneous interactions between photons and lattice phonons.[49a] As well, absorption and emission probabilities of indirect transitions are lower than for direct transitions. This explains in part the lack of observation of band edge luminescence in TiO_2 by some workers,[39,62,63] but not by others.[64] Since emission is mostly a particle surface phenomenon, luminescence quenching by the surface environment cannot be precluded in some studies.[62] Bandgap excitation of TiO_2 in vacuo yields a broad emission centered at ~2.3 eV (~500 nm; spread between 2 and 3 eV), the intensity of which is strongly affected by the presence of electron donor/acceptor molecules;[62,63] photogenerated free holes do not appear implicated in this luminescence emission.[63]

Luminescence features of TiO_2 specimens A, B, and C, recorded under otherwise identical conditions, are illustrated in Figure 6; inner-filter effects were minimized using very low TiO_2 concentrations. Appropriate control experiments disclosed that the emission features in Figure 6 are not artifacts (e.g., scattered light or Raman band of water). Emission bands from specimens A and C are less intense than those of specimen B (Figure 6b). Since excitation was carried out under equal absorption conditions at 270 nm, differences in emission intensities must originate with differences in surface properties of the various particulates. In this regard, we note that the smallest particles (2.1 nm) will likely have the larger density of surface states or defects at which nonradiative e^-/h^+ recombinations predominate. Qualitatively, the overall emission quantum yields vary as specimens B > A ~ C.

In addition to intensity differences, emission spectra also reveal differences in the number of emitting levels or centers. Estimated luminescence band maxima are collected in Table 2 in which tentative assignments are also indicated. The highest-energy emission observed under our conditions is located at about 3.83−3.85 eV and corresponds to the direct transition $\Gamma_{1b} \rightarrow \Gamma_{5'a}$ (Figure 8). The band at 3.48−3.51 eV (all samples) is the degenerate direct transition, $X_{1b} \rightarrow X_{2b}/X_{1a}$. The band edge luminescence in specimens A and B occurs at 3.20 ± 0.01 eV, while for sample C it is seen at 3.09 eV; they correspond to the highest energy *indirect trnasition* $X_{1b} \rightarrow \Gamma_3$. The lowest-energy indirect transition, also nearly degenerate $\Gamma_{1b} \rightarrow X_{2b}/X_{1a}$, is seen only for the smallest particles examined ($2R_p$ = 2.1 nm) at 2.99 eV. Additional emissions were observed at

TABLE 2: Luminescence Band Energies (eV) for TiO_2 Specimens A, B, and C

calculated energy[a]	experimental energy A	B	C	origin[b]
4.05	3.83	3.85	3.83	$\Gamma_{1b} \rightarrow \Gamma_{5'a}$
3.59, 3.45	3.48	3.51	3.48	$X_{1b} \rightarrow X_{2b}/X_{1a}$
3.19	3.21	3.19	3.09	$X_{1b} \rightarrow \Gamma_3$
3.05, 2.91	2.99			$\Gamma_{1b} \rightarrow X_{2b}/X_{1a}$
	2.79			see text
		2.69	2.67	see text
	2.56			see text

[a] Reference 51. [b] See Figure 8.

even lower energies (see Table 2) and must necessarily originate with transitions from intragap energy levels implicating lattice and/or surface defects in the particles.

Ghosh and co-workers[59] detected several defect energy levels in bulk TiO_2 rutile crystals using photoconductivity, photoluminescence excitation spectra, thermoluminescence, thermally stimulated current, electroreflectance spectra, kinetic response of the photoconductivity, and optical and thermal bleaching of electron traps. No less than eight shallow trap levels were discovered at energies from 0 to 1 eV below the conduction band (CB) at temperatures from −180 to +40 °C. At near-ambient temperature shallow traps identified with oxygen vacancies, V_O,[65−68] were established at 0.76 and 0.87 eV below CB; other workers reported shallow intragap surface states (traps) at 0.7,[69] 0.8,[70,71] and 0.9 eV[58] below CB and identified the trap with Ti^{4+} ions adjacent to oxygen vacancies.[69] This surface state was placed at 0.2 eV below CB by Hauffe et al.[71] but considerably lower (relative to CB) by others.[59]

In the emission spectral range surveyed in our study (300−500 nm), shallow trap levels were ascertained at 0.41 and 0.64 eV (sample A), 0.51 eV (sample B), and 0.53 eV (sample C) below CB of anatase (Table 2). An emission feature at 850−880 nm (~1.5 eV) reported by others in rutile[59] and anatase[62] and whose corresponding optical transition occurs at 630 nm (~2.0 eV) may be a consequence of the Franck−Condon principle and any polarizability of the lattice ions surrounding the defect; the emitting center was identified with interstitial Ti^{3+} ions.[59] Other workers suggested that the emission at ~2.0 eV originates from a level defined by an electron trapped in an oxygen vacancy[72] which Ghosh et al.[59] placed at 1.18 eV. The inference from the above discussion is that shallow traps most likely concern oxygen vacancies[73] at various energies. In this case the observed emission(s) of Figure 6 can properly be described by reactions 6−8:

$$TiO_2 \xrightarrow{h\nu} TiO_2(e^-/h^+) \rightarrow e^-_{CB} + h^+_{VB} \quad (6)$$

$$V_O^0 + e^-_{CB} \rightarrow V_O \quad \text{(electron trapping in shallow traps)} \quad (7)$$

$$V_O + h^-_{VB} \rightarrow V_O^0 + h\nu \quad \text{(radiative recombination)} \quad (8)$$

where V_O^0 (Kroger notation) is an ionized oxygen vacancy level poised to rapidly trap (in tens to hundreds of femtoseconds[74]) a photogenerated CB electron which subsequently interacts with a valence band hole (trapped in less than a few picoseconds[38]) either radiatively or nonradiatively. The dominant but not exclusive route for charge carrier recombination in small semiconductor particles is the nonradiative path because of strong coupling of wave functions of trapped electrons and trapped holes with the lattice phonons.[3]

Size Quantization in TiO_2 Particles(?). The results presented in the above sections point to the absence of size quantization for TiO_2 particles, at least at $R_p \geq 1.0$ nm. It was shown earlier that the blue shift in the absorption spectral threshold can be explained quantitatively by direct interband transitions in this genuine indirect semiconductor. The data show that conclusions about size quantization effects cannot be inferred solely on the basis of an observed blue shift of the absorption spectral edge and on an apparent satisfactory explanation of this blue shift within the framework of the effective mass approximation.[18,21,23]

The effective mass model (EMM) of small semiconductor particles, first proposed by Efros and Efros[75] and subsequently improved upon by Brus,[76] has as its main prediction that bandgaps in semiconductor particles increase with a decrease in particle dimensions. More sophisticated models have recently appeared (e.g., the tight binding model) that permit a more precise quantitative explanation of the properties of small semiconductor particles.[77−79] The appealing simplicity of the effective mass approximation and its success in qualitatively explaining the experimental data have given rise to numerous applications of the model for evaluating the exciton radius in small particles (i.e., the smallest size at which a semiconductor should display Q-size effects). Some authors have used the EMM model to quantitatively evaluate particle sizes from blue shifts in the absorption spectra. This evaluation has employed eq 1 and the assumption that the exciton effective mass (μ) of a small particle is the same as that found in bulk crystals. A priori, this assumption does not seem reasonable. The adequacy of the effective mass approximation for very small particles is unclear. The EM model overestimates the exciton kinetic energy and thus the extent to which the bandgap increases for smaller particle sizes.[78,79]

In a quantitative analysis of Q-size effects in small semiconductor particulates using the effective mass approximation, a possible increase in the exciton effective mass with decreases in particle sizes seems tempting and must be considered. The scale of such an increase may be seen by noting the results of the effective mass model application to the analysis of the data of Wang and Herron[80] on quantum size effects on the exciton confinement energy for well-characterized CdS particle sizes. This semiconductor is one of the few examples, if not the only one, for which syntheses have permitted different sized particles to be prepared and to be extensively characterized by many workers and for which good experimental data are available for scrutiny.

Figure 9 shows the dependencies of the bandgap shift as a function of the particle size of CdS calculated with eq 1 for several exciton effective masses, also calculated from eq 1 and from experimentally determined values of ΔE_{BG}.[80] It is evident that the formal use of eq 1 to estimate an effective mass gives different values of the exciton effective mass and, thus, to different dependencies of the bandgap shift on particle size. Results of these considerations show that the exciton effective mass in CdS particles for $R_p = 0.5$ nm ought to be nearly 5 times greater than that in bulk crystals (0.760 versus 0.154; see insert in Figure 9) if the EMM model and eq 1 were valid for ultrasmall particles. It must be strongly emphasized that this type of thinking results in more than a 2-fold overestimation of the particle size when eq 1 and a bulk exciton effective mass are used in particle size determination.

Although the effective mass model may qualitatively predict (at least in some cases) the direction of the spectral shift of the absorption threshold in small particles, it can lead to significantly erroneous conclusions in the quantitative estimation of particle sizes if bulk exciton effective masses are taken to apply to small particles. Its failure to quantitatively predict the extent of

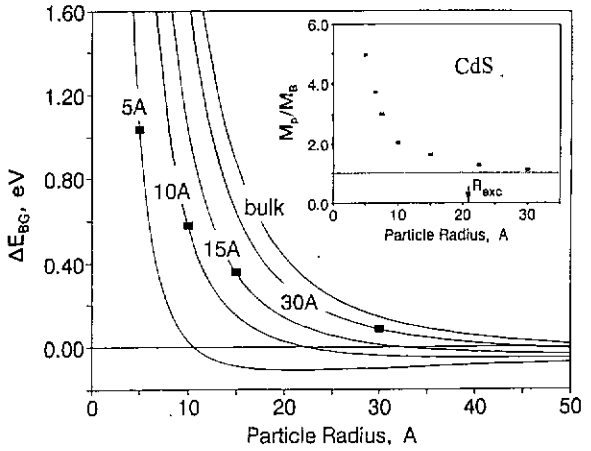

Figure 9. Family of curves plotted as change in bandgap energy versus particle radius using the effective mass model (eq 1) for various experimental radii (ref 80) and variable values of the exciton effective mass for CdS particles. Insert shows relative increase in exciton effective mass with decreasing radius in a small particle versus the corresponding exciton effective mass in a bulk crystal of CdS.

spectral blue shifts in the absorption spectra of small clusters is connected[79] with its assumptions that the effective masses of charge carriers are independent of the wave vector **k** and that the lattice structure in such clusters is the same as in bulk materials. In fact, that is intuitively not the case, particularly when the valence and conduction band levels deviate in shape from the free-electron parabolic form with such deviations being most severe for low bandgap materials like CdS, GaAs, and GaP. Calculations on titania[51] also reveal significant deviations from the parabolic form; both the valence band and the conduction band levels are rather broad and shallow. The EMM model appears satisfactory for large clusters only (several tens of angstroms), where bulk exciton effective masses may apply.

Large discrepancies exist in the reported values of bulk exciton effective mass in a TiO_2 rutile single crystal; nothing is known about TiO_2 anatase. Taking the effective mass μ of the bulk exciton for anatase to range from $\mu = 0.01m_0$[36] to $\mu \geq 3m_0$,[34] the exciton radius R_{exc} would then span $R_{exc} \sim 10^3$ nm to $R_{exc} \sim 3.2$ nm. On this basis, Q-size effects ought to be manifested in TiO_2 particles for sizes $R_p \leq 10^3$ nm (i.e., less than 1 μm) if $\mu = 0.01m_0$ and at $R_p \leq 3.2$ nm if $\mu \geq 3m_0$. Our data which indicate the absence of any size quantization effect in the TiO_2 specimens for $R_p = 1.0$ nm or greater testify that the exciton radius R_{exc} must be less than about 1.0 nm. An estimate of the effective mass of the bulk exciton using the EMM model for anatase TiO_2 would then suggest that μ must be greater than $\sim 9m_0$. The absence of good estimates of the effective masses of charge carriers in titania together with the weaknesses of the effective mass model establishes that any conclusion on size quantization effects in titania is rather premature and tenuous.

Pseudopotential band structure calculations on TiO_2 analogous to those for CdS, GaAs, GaP,[79] and Si[81] clusters using the empirical pseudopotential method (EPM) would be worth revisiting[51] to assess how cluster size would affect the optical properties of direct and indirect transitions. For CdS, the EPM model has shown that size effects are but one factor that affects absorption spectra.[79] The crystal structure (e.g., zinc blende versus hexagonal for CdS and rutile versus anatase for TiO_2), the particle shape (cubic versus spherical), and changes in the lattice constants relative to bulk lattice constants (*i.e.*, contraction of the lattice in small clusters) also contribute significantly to the exciton energies. This EPM method obviates the need for effective masses. Moreover, the calculations on GaP[79] and on Si[81] clusters predict that Franck–Condon exciton energies (direct transitions) shift blue initially and then show anomalous red shifts with decreasing cluster sizes, whereas the non-Franck–Condon exciton energies (indirect transitons) always increase (shift to blue) with decreasing cluster dimensions. The effective mass approximation model cannot account for the above effects, even qualitatively.

Conclusions

The present study examined the absorption and photoluminescence of TiO_2 colloidal particles with mean sizes $2R_p = 2.1$, 13.3, and 26.7 nm. No significant differences in absorption features were noted between the different specimens at loadings of about 15 g L^{-1}. Under our conditions, the three colloidal TiO_2 specimens displayed no size quantization (such as, e.g., blue shifts in UV-vis spectra) normally associated with decreasing particle size beyond a certain threshold. Our observations suggest that earlier reports of blue-shifted absorption thresholds, taken as evidence for Q-size effects in very small TiO_2 particles, are in fact direct (Franck–Condon type) transitions in an otherwise indirect bandgap semiconductor. Such direct transitions were noted for rutile TiO_2 crystals nearly over two decades ago.[59] Several emission bands were observed with the more intense seen in the 13.3 nm TiO_2 particles. It is interesting, but probably fortuitous, that this particle size is optimal in the derivatization of TiO_2 particulates with ruthenium complexes for use in photovoltaic devices.[82,83]

Acknowledgment. This work was sponsored by the Natural Science and Engineering Research Council of Canada. R.K. is grateful to NSERC for an award under the International Scientific Exchange Program. D.L. thanks Dr. Dani Meisel for his hospitality during a brief stay in his laboratory at Argonne National Laboratory and Mr. Liao Youxin of the Materials Science Division at Argonne for assistance with the electron microscopy and EDAX measurements. We are also grateful to Prof. J. Fendler of the University of Syracuse for the use of and Ms. Youxin Yuan for assistance with the light scattering experiments.

References and Notes

(1) For some recent reviews see for example: (a) Norris, J. R., Meisel, D., Eds. *Photochemical Energy Conversion*; Elsevier: New York, 1989. (b) Harriman, A. *Photochemistry* **1986**, *17*, 601. (c) Pelizzetti, E., Serpone, N., Eds. *Homogeneous and Heterogeneous Photocatalysis*; Reidel: Dordrecht, The Netherlands, 1986.

(2) Grätzel, M. *Acc. Chem. Res.* **1981**, *41*, 376.

(3) Grätzel, M. *Heterogeneous Photochemical Electron Transfer*; CRC Press: Boca Raton, FL, 1989.

(4) Henglein, A. *Top. Curr. Chem.* **1988**, *143*, 113.

(5) Henglein, A. *Chem. Rev.* **1989**, *89*, 1861.

(6) Kamat, P. V.; Dimitrijevic, N. M. *Sol. Energy* **1990**, *44*, 83.

(7) Brus, L. *J. Phys. Chem.* **1986**, *90*, 2555.

(8) Völz, H. G.; Kämpf, G.; Fitzky, H. G. *Farbe Lack* **1972**, *78*, 1037.

(9) As an example, see: Haase, M.; Weller, H.; Henglein, A. *J. Phys. Chem.* **1988**, *92*, 4706.

(10) As an example, see: Rossetti, R.; Ellison, J. L.; Gibson, J. M.; Brus, L. E. *J. Phys. Chem.* **1984**, *80*, 4403.

(11) As an example, see: Micic, O. I.; Meglic, M.; Lawless, D.; Sharma, D. K.; Serpone, N. *Langmuir* **1990**, *6*, 487.

(12) Henglein, A. *Ber. Bunsen-Ges. Phys. Chem.* **1982**, *86*, 241.

(13) Duonghong, D.; Ramsden, J.; Grätzel, M. *J. Am. Chem. Soc.* **1982**, *104*, 2977.

(14) Bahnemann, D.; Henglein, A.; Lillie.; Spanhel, L. *J. Phys. Chem.* **1984**, *88*, 709.

(15) Bahnemann, D.; Henglein, A.; Spanhel, L. *Faraday Discuss. Chem. Soc.* **1984**, *78*, 151.

(16) Howe, R. F.; Grätzel, M. *J. Phys. Chem.* **1985**, *89*, 4495.

(17) Nozik, A. J. In *Photocatalytic Purification and Treatment of Water and Air*; Ollis, D. F., Al-Ekabi, H., Eds.; Elsevier Science Publishers: Amsterdam, 1993; pp 39–48.

(18) Kormann, C.; Bahnemann, D. W.; Hoffmann, M. R. *J. Phys. Chem.* **1988**, *92*, 5196.
(19) Bahnemann, D. W. *Isr. J. Chem.* **1993**, *33*, 115.
(20) Kavan, L.; Stoto, T.; Gratzel, M.; Fitzmaurice, D.; Shklover, V. *J. Phys. Chem.* **1993**, *97*, 9493.
(21) Anpo, M.; Shima, T.; Kodama, S.; Kubokawa, Y. *J. Phys. Chem.* **1987**, *91*, 4305.
(22) Joselevich, E.; Willner, I. *J. Phys. Chem.* **1994**, *98*, 7628.
(23) Choi, W.; Termin, A.; Hoffmann, M. R. *J. Phys. Chem.* **1994**, *98*, 13669.
(24) Fox, M. A. *Top. Curr. Chem.* **1987**, *142*, 71.
(25) Matthews, R. W. *Sol. Energy* **1987**, *38*, 405.
(26) Ollis, D. F. *Environ. Sci. Technol.* **1985**, *19*, 480.
(27) Nishimoto, S.-I.; Ohtani, B.; Shirai, H.; Adzuma, S.; Kagiya, T. *Polym. Commun.* **1985**, *26*, 292.
(28) Duonghong, D.; Ramsden, J.; Gratzel, M. *J. Am. Chem. Soc.* **1982**, *104*, 2977.
(29) Moser, J.; Gratzel, M. *J. Am. Chem. Soc.* **1982**, *104*, 2977.
(30) (a) Pankove, J. I. *Optical Processes in Semiconductors*; Dover: New York, 1971. (b) Liu, C.; Bard, A. J. *J. Phys. Chem.* **1989**, *93*, 3232.
(31) Acket, G. A.; Volger, J. *Physica (Amsterdam)* **1966**, *32*, 1680.
(32) Pascual, J.; Camassel, J.; Mathieu, H. *Phys. Rev. B: Condens. Matter* **1978**, *18*, 5606.
(33) Agekyan, V. T.; Berezhnaya, A. A.; Lutsenko, V. V.; Stepanov, Y. A. *Sov. Phys. Solid State* **1980**, *22*, 6.
(34) Kasinski, J. J.; Gomez-Jahn, L. A.; Faran, K. J.; Gracewski, S. M.; Miller, Dwyane, R. J. *J. Chem. Phys.* **1989**, *90*, 1253.
(35) Boudreaux, D. S.; Williams, F.; Nozik, A. J. *J. Appl. Phys.* **1980**, *51*, 2158.
(36) Yahia, J. *Phys. Rev.* **1963**, *130*, 1711.
(37) Lawless, D. Ph.D. Thesis, Concordia University, Montreal, Canada, 1993.
(38) Serpone, N.; Lawless, D.; Khairutdinov, R.; Pelizzetti, E. *J. Phys. Chem.* **1995**, *99*, 16655.
(39) Moser, J. Ph.D. Dissertation, Thesis No. 616, Ecole Polytechnique Fédérale de Lausanne, Lausanne, Switzerland, 1986.
(40) Ciavatta, L.; Ferri, D.; Riccio, G. *Polyhedron* **1985**, *4*, 15.
(41) Sclafani, A.; Palmisano, L.; Schiavello, M. *J. Phys. Chem.* **1990**, *94*, 829.
(42) Serpone, N. Ph.D. Thesis, Cornell University, Ithaca, NY 1968.
(43) Serpone, N.; Kennepohl, P. Unpublished observations (from P. Kennepohl, Senior Undergraduate Thesis, Concordia University, Montreal, Canada, Dec 1992).
(44) Cullity, B. A. *Elements of X-ray Diffraction*; Addison-Wesley: London, 1956.
(45) Sproull, W. T. *X-Rays in Practice*; McGraw-Hill: New York, 1946; p 430.
(46) Choi, W.; Termin, A.; Hoffmann, M. R. *Angew. Chem., Int. Ed. Engl.* **1994**, *33*, 1091.
(47) In the assessment of this 150 meV for the colloids prepared by hydrolysis of $TiCl_4$, it was assumed (ref 19) that the corresponding colloids made from hydrolysis of $Ti(O-CH(CH_3)_2)_4$ possessed the bandgap of bulk anatase TiO_2 (3.2 eV). Conclusions that the bandgap shift is indicative of quantum size effects for particles of ~20 Å size must be taken with some reservations.
(48) Delgass, W. N.; Haller, G. L.; Kellerman, R.; Lunsford, J. H. *Spectroscopy in Heterogeneous Catalysis*; Academic Press: New York, 1979; p 128.
(49) (a) Mooser, E.; Pearson, W. B. In *Progress in Semiconductors*; Gibson, A. F., Ed.; John Wiley & Sons: New York, 1960; Vol. 5, p 53. (b) Zhao, X. K.; Fendler, J. H. *J. Phys. Chem.* **1991**, *95*, 3716.
(50) Salvador, P. *Sol. Energy Mater.* **1982**, *6*, 241.
(51) Daude, N.; Gout, C.; Jouanin, C. *Phys. Rev. B* **1977**, *15*, 3229.
(52) Gallay, R.; van der Klink, J. J.; Moser, J. *Helv. Chim. Acta* **1985**, *58*, 805.
(53) Huckel, W. *Structural Chemistry of Inorganic Compounds*; Elsevier: Amsterdam, 1951; Vol. II, pp 678–685.
(54) Breckenridge, R. G.; Hosler, W. R. *Phys. Rev.* **1953**, *91*, 793.
(55) Kahn, A. H.; Leyendecker, A. J. *Phys. Rev.* **1964**, *135*, A1321.
(56) Arntz, F.; Yacoby, Y. *Phys. Rev. Lett.* **1966**, *17*, 857.
(57) Vos, K.; Krusemeyer, *Solid State Commun.* **1975**, *15*, 949.
(58) Frova, A.; Body, P. J.; Chen, Y. S. *Phys. Rev.* **1967**, *157*, 157.
(59) Ghosh, A. K.; Wakim, F. G.; Adiss, Jr., P. R. *Phys. Rev.* **1969**, *184*, 979.
(60) Cardona, M.; Harbeke, G. *Phys. Rev.* **1965**, *137*, 1467.
(61) Koffyberg, F. P.; Dwight, K.; Wold, A. *Solid State Commun.* **1979**, *30*, 433.
(62) Forss, L.; Schubnell, M. *Appl. Phys.* **1993**, *B56*, 363.
(63) Hashimoto, K.; Hiramoto, M.; Sakata, T. In *Photoelectrochemistry and Electrosynthesis on Semiconductor Materials*; The Electrochemical Society: Pennington, NJ, 1988; Vol. 88–14, pp 395–400.
(64) Chandrasekaran, K.; Thomas, J. K. *J. Chem. Soc., Faraday Trans. 1* **1984**, *80*, 1163.
(65) Chester, P. F. *J. Appl. Phys.* **1961**, *32*, 2233.
(66) Bogomolov, V. N.; Sochava, L. S. *Sov. Phys. Solid State* **1968**, *9*, 2647.
(67) (a) Weeks, R. A.; Purcell, T. *Bull. Am. Phys. Soc.* **1968**, *13*, 435. (b) Purcell, T.; Weeks, R. A. *Am. Ceram. Soc. Bull.* **1968**, *47*, 757.
(68) Jingsbury, Jr., P. I.; Ohlsen, W. D.; Johnson, O. W. *Phys. Rev.* **1968**, *175*, 1091.
(69) Redmond, G.; Fitzmaurice, D.; Gratzel, M. *J. Phys. Chem.* **1993**, *97*, 6951.
(70) Siripala, W.; Tomkievicz, M. *J. Electrochem. Soc.* **1982**, *129*, 1240.
(71) Hauffe, K.; Hupfeld, J.; Wetterling, J. *Z. Phys. Chem. (Munich)* **1976**, *103*, 115.
(72) (a) Confova, P.; Arend, H. *Czech. J. Phys.* **1961**, *B11*, 416. (b) Dvorak, V. *Czech. J. Phys.* **1961**, *B11*, 253.
(73) Lu, G.; Linsebigler, A.; Yates, Jr., J. T. *J. Phys. Chem.* **1994**, *98*, 11738.
(74) Colombo, Jr., D. P.; Roussel, K. A.; Saeh, J.; Skinner, D. E.; Bowman, R. M. *Chem. Phys. Lett.* **1995**, *232*, 207.
(75) Efros, Al. L.; Efros, A. L. *Fiz. Tekh. Poluprovodn.* **1982**, *16*, 1209 {*Sov. Phys.-Semicond.* **1982**, *16*, 772}.
(76) Brus, L. E. *J. Chem. Phys.* **1984**, *80*, 4403.
(77) Wang, Y.; Suna, A.; Mahler, W.; Kasowski, R. *J. Chem. Phys.* **1987**, *87*, 7375.
(78) Lippens, P. E.; Lannoo, M. *Phys. Rev. B* **1989**, *39*, 10935.
(79) Rama Krishna, M. V.; Friesner, R. A. *J. Chem. Phys.* **1991**, *95*, 8309.
(80) Wang, Y.; Herron, M. *Phys. Rev. B* **1990**, *42*, 7253.
(81) Rama Krishna, M. V.; Friesner, R. A. *J. Chem. Phys.* **1992**, *96*, 873.
(82) Grätzel, M. In *Photochemical Energy Conversion*; Norris, J. R., Meisel, D., Eds.; Elsevier: New York, 1989.
(83) Vlacopoulos, N.; Liska, P.; Augustynski, J.; Grätzel, M. *J. Am. Chem. Soc.* **1988**, *110*, 1216.

JP9503167